(Received 11 December 2025, Accepted 21 February 2026, Scheduled 10 May 2026)

# Noninvasive Brain Tumor Detection Using a Frequency Selective Surface Gain Enhanced Antenna

Sanjeev Sharma[1], Daljeet Singh[2, 3, 6], Mariella Särestöniemi[2, 3, 4], Teemu Myllylä[2, 3, 5], and Rajeev Kumar[7, *]

[1] University School of Research, Rayat Bahra University, Kharar, Punjab-140103, India
[2] Research Unit of Health Sciences and Technology, Faculty of Medicine, University of Oulu, Oulu 90570, Finland
[3] Infotech Oulu, 90570, Finland
[4] Centre for Wireless Communications, Faculty of Information Technology and Electrical Engineering, University of Oulu, Finland
[5] Opto-Electronics and Measurement Technique Research Unit, Faculty of Information Technology and Electrical Engineering University of Oulu, Finland
[6] School of Electronics and Electrical Engineering, Lovely Professional University, Punjab, India
[7] Chitkara University Institute of Engineering and Technology, Chitkara University, Punjab, India

**ABSTRACT:** This article introduces a microwave system operating in the low-frequency band of 1.6–2.8 GHz, specifically designed for biomedical applications. Tumor detection in the human brain was achieved by monitoring variations in antenna $S$-parameter response. A high-gain antenna was positioned on the skull's surface, whose gain and directivity are enhanced by backing it with a Frequency Selective Surface (FSS) array. This arrangement effectively channels energy toward human tissues, which facilitates tumor detection. The combined Antenna-FSS structure improved the gain and directivity by 5.3 and 5.1 dB, respectively. Simulations were conducted using a multilayered skull model consisting of the skin, skull, and brain. The experimental validation was done by performing measurements using a near-realistic human brain phantom and by inserting a tumor in the brain area of the fabricated phantom. The study revealed that the measured $S$-parameters vary by approximately 11.38 dB when a 6 mm $\times$ 6 mm tumor is introduced into the brain region. Additionally, $S$-parameters are analysed by varying shapes, sizes, and locations of tumors within the brain. The study's findings indicate that variations in the characteristics of the $S$-parameter can be potentially utilized for detecting tumors in the human brain.

## 1. INTRODUCTION

Brain tumors and other brain-related diseases have made a massive impact on healthcare in recent years, becoming leading causes of disability and death. Among humans, brain tumors are known to be the 9th leading cause of death [1]. When an individual is affected by a brain tumor, it may cause irreversible impairment of the overall brain's cognition and health. Hence, it is crucial to diagnose and treat these tumors in a timely manner. If not treated, these tumors can cause abnormal cell development inside the brain, thus transforming into Brain Cancer. Tumors can be either benign or malignant. The former is a non-cancerous form of tumor, which means that it does not harm other parts of the body. The latter is the cancerous form which occurs when benign tumors transform into malignant tumors by spreading across vital organs in the body, affecting their functionality. However, timely diagnosis and proper treatment can help improve the chances of survival of the patient [2]. With the evolution of research in the medical field, modalities like ultrasound, computed tomography (CT), X-ray imaging, magnetic resonance imaging (MRI), biopsy, positron emission tomography (PET) scans, etc. have been proposed for diagnosis. These techniques have drawbacks, including high cost, labor-intensive processes, and the need for extensive hardware, restricting their use in specialized hospitals. Conversely, in time-critical situations and locations lacking the above modalities, microwave techniques have proved to be more effective [3]. These systems are regarded as suitable due to their low power consumption, planar low-profile structures, non-ionizing characteristics, and cost-effectiveness, which enable deeper penetration into the body [4–6]. For brain tumor treatment, the technique of Microwave Hyperthermia is employed [7–10]. Additionally, microwaves are used for tumor diagnosis in other regions of the body as well, such as the breasts [11, 12], lungs [13], and other areas [14–16].

For brain imaging applications, Rodriguez et al. [17] presented a brick-shaped antenna that was tested on head phantom models and operated at 800 MHz–1.2 GHz. For a similar use case, the authors in [18] fabricated a multilayer metamaterial-based antenna array using Rogers RT5880 and RO4350B substrates with nine elements in each array. In another work on brain tumor diagnosis, Hamza et al. [19] used an artificial magnetic conductor with a resonant frequency of 2.276 GHz and embedded it in their proposed microwave system. The authors in [20] used a deep transfer learning model to classify brain tumors instead of metamaterial-based solutions. Their model consisted of five layers, and when tested on a dataset with 4200 images, it achieved an accuracy of 99.65% and an F-score of 99.23%.

* Corresponding author: Rajeev Kumar (rajeev.kumar@chitkara.edu.in).

The authors of [21] used $S$-parameter analysis to create a slotted microstrip patch antenna operating at 6–10 GHz for brain tumor diagnosis. The testing results for its specific absorption rate (SAR) were found to be $2.53 \times 10^6$ W/m$^3$. In another work, Chandra and Balasingham [22] presented a microwave system operating at the 403.5 MHz band based on finite-difference-time-domain (FDTD) simulation. In this work, the authors demonstrate that for diagnosing small-sized tumors, a threshold signal-to-noise ratio (SNR) of 45 dB is crucial. In [23], the authors tested a microwave system with a bandwidth of 1.59 to 5.2 GHz in Computer Simulation Technology (CST) Microwave Studio using simulations on a seven-layer model. Digital Twins (DTs) using microwave systems were proposed by Särestöniemi et al. [6] for brain tumor detection. Based on user specifications, these DTs can be tailored to accommodate specific cases of brain tumor size, location, and severity.

In [24], the authors presented 3D emulation models for microwave system evaluation under different conditions, such as tumors, strokes, and cancers. Groumpas et al. proposed a near-field microwave radiometry system operating at 1.5 GHz [25] for passive brain tumor detection. At the core of this system is a four-port total power Dicke switch. In another study [26], the authors used reconstructed microwave brain (RMB) images with overall six different classes of tumors as reference cases for brain tumor classification.

The present work introduces a microwave system for noninvasively detecting the existence of tumors in the human brain. The presented antenna system radiates at a low frequency band of 1.6–2.8 GHz. The novel technique leverages variations in the antenna responses to detect the tumor. To achieve precise real-time diagnosis, a high-gain antenna was placed on the surface of the skull. A uniquely designed Frequency Selective Surface (FSS) array structure is positioned behind the antenna to channelize the energy towards the human tissues to improve the antenna gain by 5.3 dB and directivity by 5.1 dB. Simulation results for the proposed system obtained by realistic digital twin multilayer skull models, comprising the Skin, Skull, and Brain, show that even extremely small tumors of any shape can be diagnosed accurately.

The antenna parameters, such as gain and directivity, are substantially improved by deploying a uniquely designed Frequency Selective Surface (FSS) array structure, which was placed behind the antenna [27]. The FSS array was used to direct the electromagnetic energy towards the human tissues. The use of the FSS structure improves the antenna gain by 5.3 dB and directivity by 5.1 dB. A multilayer skull model, which comprises Skin, Skull, and Brain, is used for simulation purposes. The simulated results attained by the use of near-realistic digital twin models of the human head illustrate that the proposed microwave system can be used to detect even small-sized tumors of any random shape with high accuracy.

The rest of the paper is organized as follows. In Section 2, the microwave system design utilized in this work is presented. It also includes antenna and FSS unit cell structures. Section 3 discusses the characteristics of the proposed antenna for various tumor shapes. Section 4 explores measurements using a near-realistic brain phantom. Finally, Sections 5 and 6 provide a comparison and concluding remarks, respectively.

## 2. ANTENNA DESIGN

The antenna design uses a Roger RT/Duroid 5880 substrate with a thickness of 0.51 mm and dimensions of 44 mm $\times$ 40 mm. The lower part of the feedline had dimensions of 13 mm $\times$ 2.2 mm, and a semi-circle of 10 mm radius is placed on the top of this feedline. Two rectangular structures with sizes of 7 mm $\times$ 8 mm and 3 mm $\times$ 6 mm were placed above the semi-circle as shown in Figure 1. The top part of the feedline has a thin line of 0.5 mm width and 7 mm length, which precisely aligns with the ground plane as shown in Figure 1. The sides of the substrate are further extended by 4 mm on either side to accommodate the screws for holding the separating rods, which are used to firmly position the FSS and antenna separation.

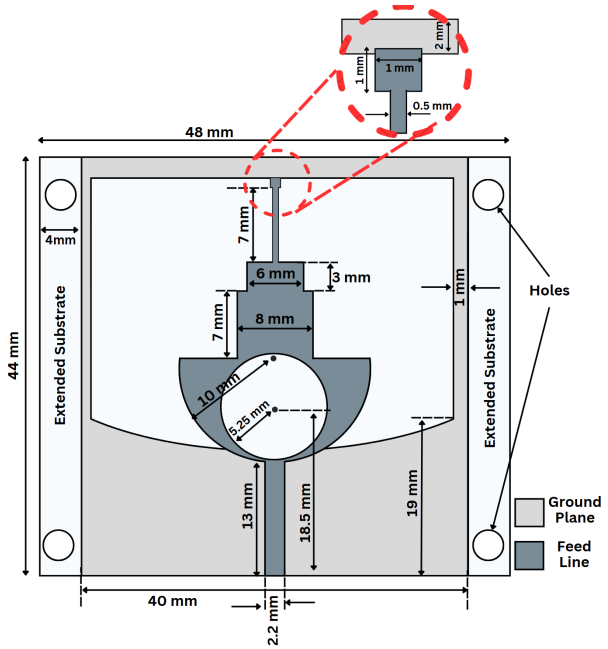


**FIGURE 1**. Antenna design.

**FSS unit cell:** The FSS unit cell with dimensions of 15 mm $\times$ 15 mm $\times$ 1.6 mm is designed on an FR4 substrate. The unit cell consists of an outer square of 14.6 mm $\times$ 14.6 mm. An inner square of dimension 13 mm $\times$ 13 mm is etched out from the outer square as shown in Figure 2(a).

The simulation was performed using ANSYS HFSS software by simulating a two-port Floquet configuration, as shown in Figure 2(b). The FSS array was designed to cover the required bandwidth of the intended application along with an acceptable return loss. As discussed in further sections, a frequency range of approximately 2 GHz to 3 GHz will be used to detect tumors. Therefore, both the FSS array and antenna are required to radiate in the mentioned frequency band. The operating frequency band of less than 3 GHz was selected based on a trade-off between penetration depth, spatial resolution, and overall size of antenna. At lower frequencies, there is a greater penetration of RF-waves in the lossy body tissues. However, spatial resolution is better at higher frequencies but has poor penetration.

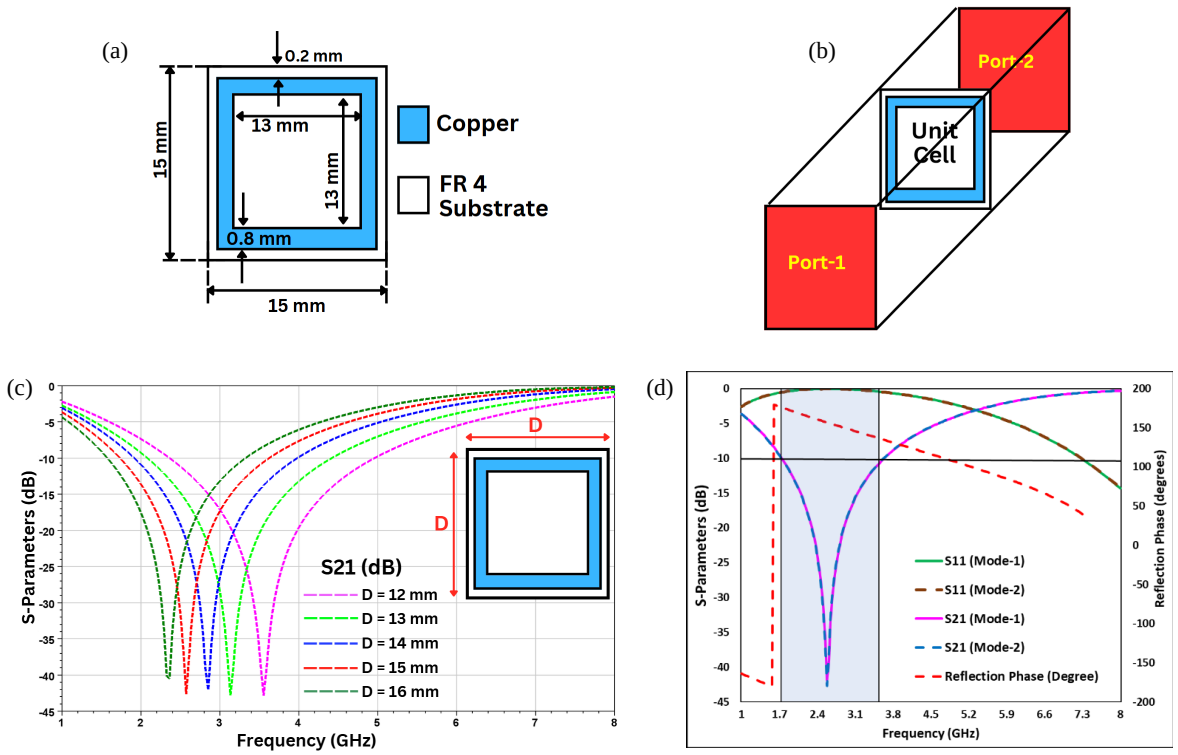


**FIGURE 2**. FSS unit cell design: (a) unit cell dimensions, (b) simulation setup, (c) optimisation with cell width, (d) $S$-parameters.

Also, at lower frequencies, the antenna size tends to increase. For a brain tumor monitoring application, greater penetration is required for multilayered brain tissues; therefore, frequency band of 2–3 GHz was selected. Further lowering the operating band will make the antenna size larger and will lead to poor spatial resolution, which will make it less suitable for practical applications.

The dimensions of the square-shaped unit cell were optimised to cover the mentioned band by varying the outer side ($D$) from 12 mm to 16 mm, as shown in Figure 2(c). As the size of the square FSS was increased, the $S_{21}$ curve shifted to a lower band. With an optimal size of $D = 15$ mm, the $S_{21}$ curve gets centered at about 2.6 GHz, which covers the entire 2–3 GHz band.

As shown in Figure 2(c), the FSS unit cell is designed so that $S_{21}$ characteristics deliver a wide frequency range covering 1.7 GHz to 3.7 GHz with a centre frequency at 2.6 GHz. This indicates that electromagnetic waves that are incident on the surface of the Frequency Selective Surface (FSS) within this frequency range are reflected back. These reflected waves interfere constructively with the incoming waves, resulting in an enhanced signal. Consequently, this supports channelizing the antenna's electromagnetic energy in a particular direction, which leads to improvements in several antenna parameters, for example, gain, directivity, and front-to-back ratio (FTBR). The reflection phase of the FSS unit cell is another important parameter for enhancing the performance of the antenna. The reflection phase should linearly decrease in the operational band so as to provide the required phase reflection [28]. As seen in Figure 2(d), the reflection phase decreases linearly in the highlighted frequency band.

The designed single FSS unit cell was repeated several times to form the FSS array. An array of $8 \times 6$ unit-cells was created with an overall size of 120 mm $\times$ 90 mm as depicted in Figure 3. Each unit cell was separated from the adjoining unit cell by a distance of 0.4 mm. Additionally, four holes were drilled in the FSS array, which was used to hold the separating rods between the FSS and antenna.

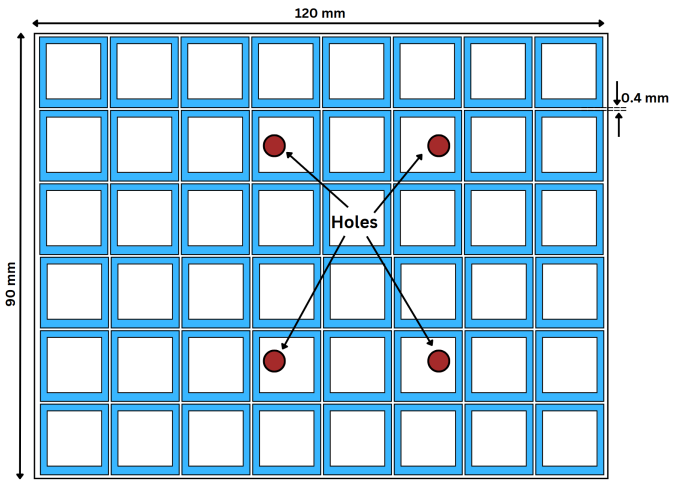


**FIGURE 3**. FSS array.

**Combined FSS array and Antenna setup**: The FSS array surface was placed 10 mm above the antenna feed plane surface as shown in Figure 4. With the combined use of antenna and FSS array, several antenna parameters were enhanced [29]. To provide a physiological context for the proposed antenna-based sensing approach, the dielectric properties of brain tis-

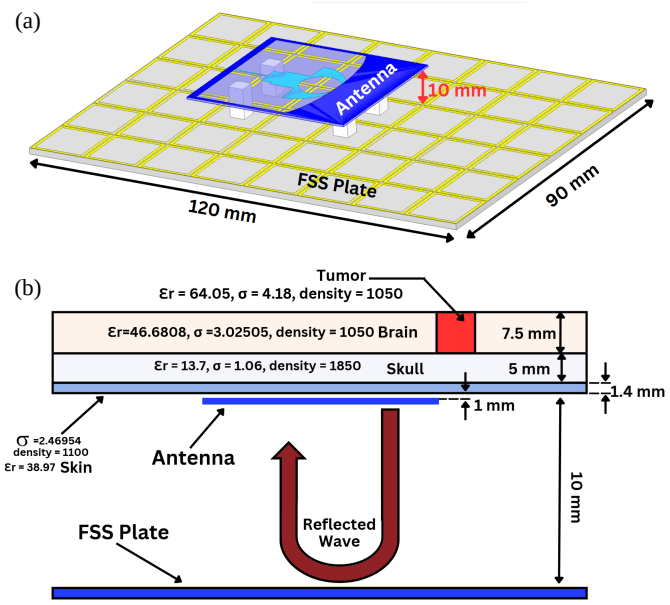


**FIGURE 4**. Combined structure: (a) 3-D view, (b) side view.

sues and tumors were incorporated into the electromagnetic modeling for the 2–4 GHz frequency range, as shown in Figure 4(b). Within this band, healthy brain tissues (such as grey matter) typically exhibit a relative permittivity of $\varepsilon_r \approx 38$–$46$ and conductivity $\sigma \approx 1.2$–$2.0$ S/m. In contrast, malignant tumor tissues generally possess higher water content, which leads to elevated dielectric properties with $\varepsilon_r \approx 45$–$65$ and conductivity $\sigma \approx 1.5$–$2.5$ S/m across this frequency range.

The dielectric contrast between the tumor and the surrounding healthy tissue produces localized electromagnetic scattering and impedance mismatch when illuminated by the antenna. As a result, the presence of a tumor induces measurable variations in the reflection coefficient ($S_{11}$) and transmission coefficient ($S_{21}$). These variations are observed in the form of resonance frequency shifts and amplitude variations. Larger tumors or tumors with greater dielectric contrast produce stronger scattering effects, which lead to more significant changes in $S$-parameter magnitude and phase. On the other hand, smaller or irregularly shaped tumors result in smaller variations due to reduced scattering cross-section and distributed field interaction.

Figure 5(a) depicts the radiation patterns at 2.25 GHz for both configurations, the antenna alone and the antenna combined with the Frequency Selective Surface (FSS). A clear enhancement in gain is observed when the FSS is integrated with the antenna, which demonstrates its constructive impact on radiation performance. Figure 5(b) compares the measured and simulated radiation patterns, which show close agreement and validates the design accuracy.

As shown in Figure 5(c), the simulated gain increases significantly from 3.3 dB to 8.6 dB with the integration of the FSS plate with the antenna. Likewise, Figure 5(d) shows that the simulated directivity improves from 3.6 dB to 9.1 dB. This improvement was due to the ability of the FSS to reflect and refocus the radiated electromagnetic energy in a specific direction, which results in stronger forward radiation, deeper tissue penetration, and enhanced tumour detection capability. Figure 5(c) also shows the measured values of gain and directivity, with peak measured values of Gain and Directivity of 8.3 and 8.9 dB, respectively.

$S_{11}$ characteristics can be understood under three different conditions (Cases) as listed below.

**Case-1 (With Antenna and FSS combination)**: As shown in Figure 6, the $S_{11}$ plot for the Antenna and FSS combination shows resonance at two different frequencies, one at 2.8 GHz and the other at 4.1 GHz.

**Case-2 (With Antenna, FSS, and human body):** When the Antenna-FSS combination was placed at 1 mm separation from the body (as shown in Figure 4), there was a shift in resonance frequency from 2.8 GHz to 2.2 GHz. In addition, the $S_{11}$ plot showed a wide bandwidth.

**Case-3 (With Antenna, FSS, Human body with Tumor):** In this scenario, a spherically shaped tumor of radius 3.5 mm was inserted in the brain area as shown in Figure 4. It is observed that when the tumor is aligned at the position depicted in Figure 4(b) and Figure 6 (inset), the combined structure resonates sharply at approximately 2.3 GHz frequency with $-36.3$ dB return loss. This sharp variation in the $S_{11}$ characteristics can potentially be exploited to detect the presence of a tumor inside the human brain.

A large change in the $S_{11}$ characteristics with tumor insertion is due to a change in the dielectric environment surrounding the FSS-Antenna sensor. As depicted earlier in Figure 4(b), the dielectric properties of the tumor are much higher than those of the surrounding brain tissues; any addition of the tumor in the brain area changes the overall dielectric environment. This causes variation in the electromagnetic field distribution of the sensor, which leads to a change in sensor response. This variation in sensor response gets further enhanced due to FSS integration, as the electromagnetic energy becomes more directed towards the brain tissues. Therefore, any change in the overall dielectric environment due to tumor insertion causes enhanced variation in sensor response characteristics.

Case-3, described above, was further tested by varying the distance (Dist) of the placement of the antenna from the Skull surface, as shown in Figure 7. As the distance was increased from 1 mm to 5 mm, the dip in the $S_{11}$ curve slightly decreases gradually, along with a shift in the resonant frequency. However, the difference between the notch level depth and the "No Tumor" case is large enough to reliably indicate the presence of a tumor.

**SAR Evaluation and Safety Compliance:** The specific absorption rate (SAR) parameter is used to assess the health risk associated with the exposure of electromagnetic waves on human tissues. SAR is evaluated as per below formula [30, 31]:

$$SAR = \frac{\sigma \left|\vec{E}\right|^2}{\rho}$$

where $\rho$ (kg/m$^3$) is the mass density of the tissue, and $\sigma$ (S/m) is its conductivity. The value of the applied electric field strength is represented by $E$ (V/m).

The 10-g SAR results evaluated at 2.23 GHz frequency using port excitation with 40 mW input power are shown in Fig-

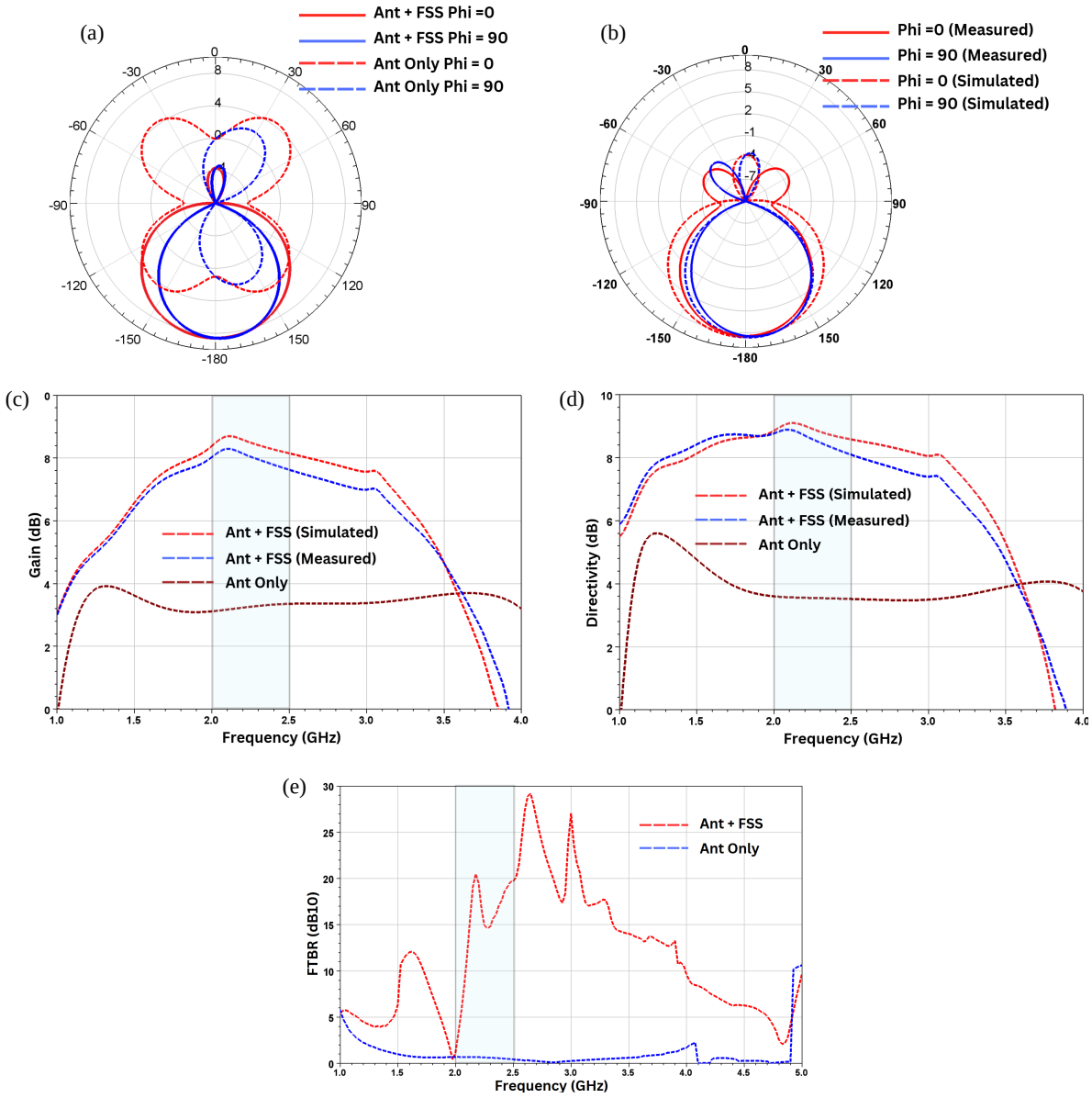


**FIGURE 5**. Combined antenna and FSS characteristics, (a) radiation pattern at 2.25 GHz, (b) gain, (c) directivity, (d) FTBR.

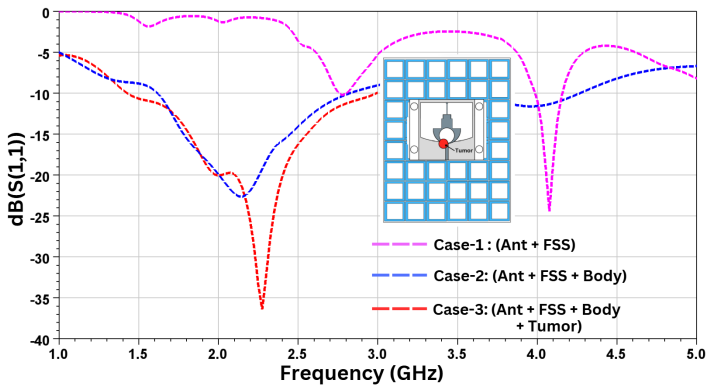


**FIGURE 6**. $S_{11}$ characteristics.

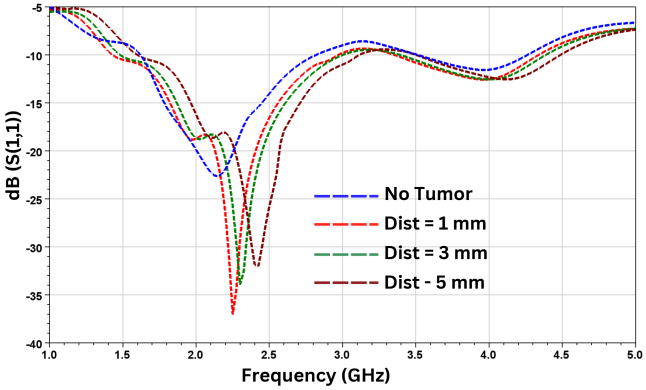


**FIGURE 7**. Variation with distance (Dist) of Antenna from Skull Surface.

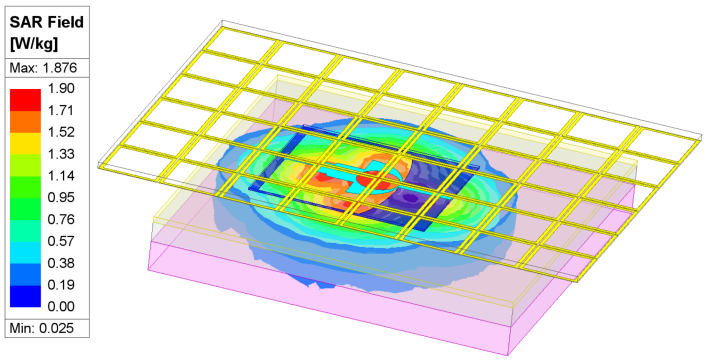


**FIGURE 8**. SAR analysis.

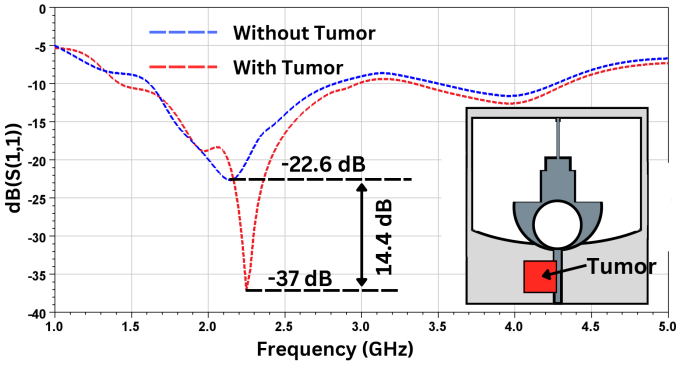


**FIGURE 9**. Cube-shaped tumor.

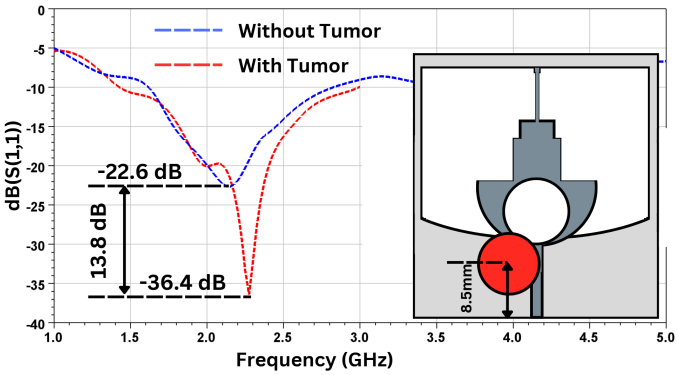


**FIGURE 10**. Sphere-shaped tumor.

ure 8. When the skull surface is kept at 1 mm distance from the antenna, the peak 10 g averaged SAR was found to be 1.876 W/kg. This value is within the IEEE general prescribed limit of 2 W/kg [30]. Since SAR scales linearly with input power, the proposed sensing configuration can be safely operated within regulatory limits under controlled diagnostic conditions. Additionally, the system is intended only for short-duration tumor detection rather than continuous wearable operation.

## 3. *S*-PARAMETER VARIATION WITH DIFFERENT TUMOR SHAPES

In this section, three different shapes of tumors were used to simulate the $S$-parameters. The purpose was to confirm that there should be sufficient variation in $S$-parameters when a tumor is inserted into the brain area. Although real-world actual tumors may be of irregular shape and varying size, for simulation purposes, we used three available geometric shapes. The results are as follows:

a) **Cubical-shaped tumor** — A tumor of size 6 mm × 6 mm × 7.5 mm was placed in the brain area at a specific location as shown in Figure 9. The $S_{11}$ plot, which earlier showed a dip of $-28.5$ dB without a tumor, now shows a sharp dip of $-37$ dB. A variation of 8.5 dB in $S_{11}$ with and without a tumor is sufficient to indicate the presence of a tumor.

b) **Spherical-shaped tumor** — A sphere-shaped tumor of radius 3.5 mm was inserted at the location shown in Figure 10. The $S_{11}$ showed a decrease of 7.8 dB, which indicates the tumor presence.

c) **Cylindrical-shaped tumor** — As displayed in Figure 11, a tumor with a cylindrical shape of radius 3.5 mm and length 8 mm was placed, which decreases the $S_{11}$ curve to $-34.7$ dB. There is a variation of 6.2 dB, which is adequate enough to suggest the presence of a tumor.

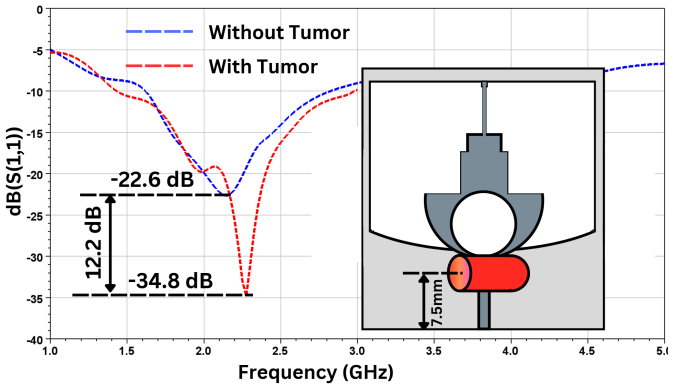


**FIGURE 11**. Cylinder-shaped tumor.

### 3.1. Tumor Size Effect on *S*-Parameters

Not only the shape, but the tumor size also has an impact on the $S$-parameter response. Larger tumors generate a larger dip in

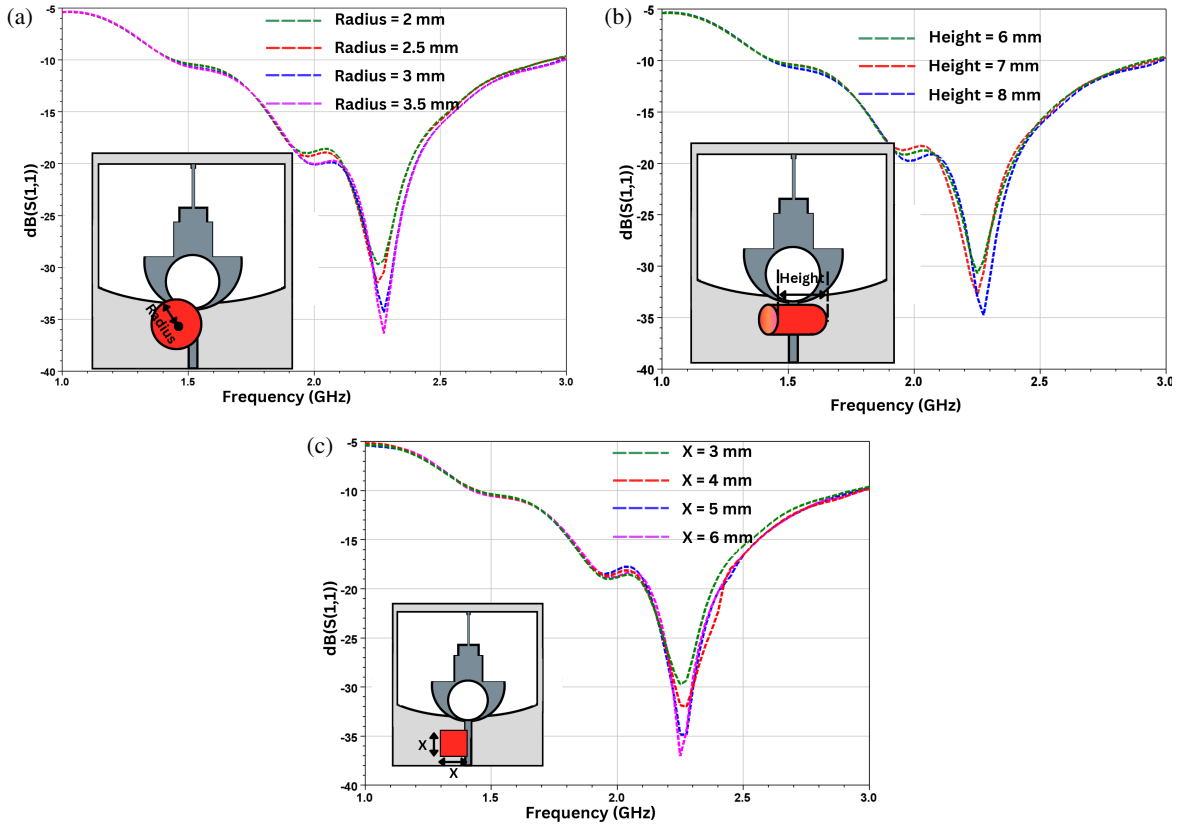


**FIGURE 12**. Variation with the size of tumor: (a) spherical tumor, (b) cylindrical tumor, (c) cubical tumor.

the $S_{11}$-curve. The response curve indicates that the proposed sensor not only indicates the presence of a tumor but can also be used to estimate its size. This $S_{11}$ response demonstrates a clear relationship between tumor size and the observed $S$-parameter variations, which highlights the sensor's ability to not only detect tumors but also estimate their size. This functionality has significant clinical value as it enables continuous and noninvasive monitoring of the progression or shrinkage of the tumor over time, which makes the proposed microwave sensing system a promising tool for both diagnosis and follow-up assessments in medical applications.

As depicted in Figure 12(a), increasing the radius of the spherical tumor from 2 mm to 3.5 mm results in a deepening of the $S_{11}$ notch, which indicates stronger interaction with the electromagnetic field. A similar trend is observed for the cylindrical tumor in Figure 12(b), where an increase in the height of the cylinder from 6 to 8 mm leads to a deeper notch response. Likewise, for the cubical tumor shown in Figure 12(c), enlarging the cube's dimensions produces an increase in the notch depth, which confirms the consistent sensitivity of the proposed sensor to variations in the tumor size across different geometrical shapes.

## 4. TRIALS WITH PHANTOM MIMICKING HUMAN BRAIN AND FABRICATED SENSOR DESIGN

To verify the simulation results, a measurement setup was created to mimic a realistic scenario. The sensor was fabricated, as shown in Figure 13(a) depicting the feed plane side of the antenna design fabricated using a Rogers RT/Duroid 5880 substrate. Figure 13(b) shows the FSS plate with an array of square units fabricated on an FR4 substrate. Figure 13(c) shows the combined Antenna and FSS plate, which were firmly secured to each other using Teflon rods and screws. The proposed sensor was tested on a phantom model that mimicked the human brain and was fabricated using the procedure described in [24, 32]. Two brain phantom models were created, one without any tumor or abnormalities, and the second model was inserted with a tumor of approximate size $6 \times 6 \times 6\,\text{mm}^3$. The dielectric parameter values of the brain tissues used in the model for the operating frequency band of 2–4 GHz were selected based on well-established experimental databases of biological tissues at microwave frequencies [33, 34] and are summarized in Table 1.

The measurement setup of the fabricated sensor and brain phantom was created as shown in Figures 14(a) and (b). Two sets of measurement readings with a Vector Network Analyzer (VNA) were performed: one with a healthy brain phantom (without any abnormalities), and the other with a tumorous phantom. The $S$-parameter response of the sensor was captured for both scenarios and is plotted in Figure 14(c). It is observed that:

a) For testing with a healthy phantom, the $S_{11}$-Curve shows a notch level of $-22.62$ dB at 2.9 GHz.

b) With the tumoric phantom, the $S_{11}$-curve has a notch level deepening to $-34$ dB at 2.7 GHz.

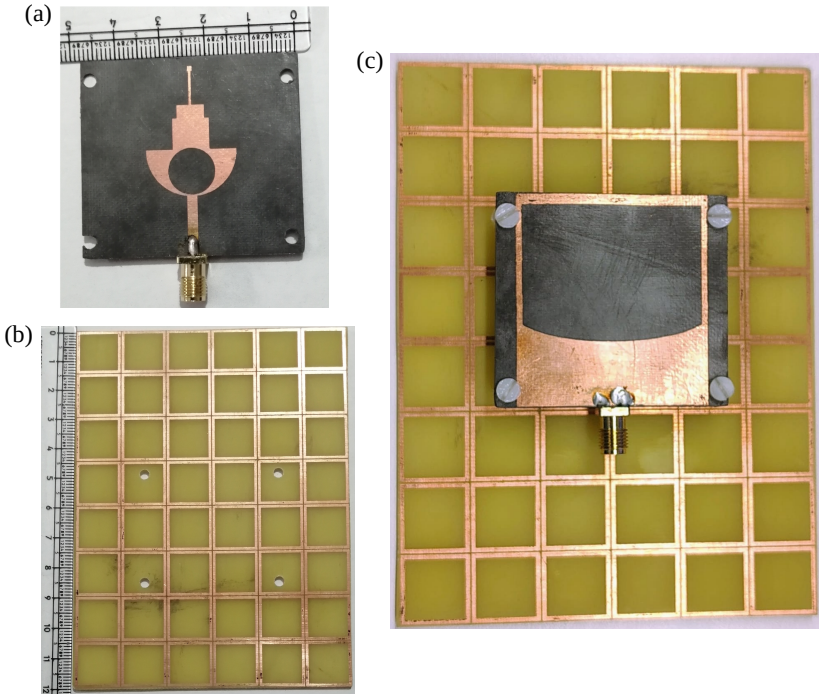


**FIGURE 13**. Fabricated images: (a) antenna (Feed Side), (b) FSS plate, (c) combined structure.

**TABLE 1**. Dielectric values of tissue layers.

| Tissue Layer Name | Thickness (mm) | Simulation Values | | Phantom Values | |
|---|---|---|---|---|---|
| | | $\varepsilon_r$ | $\sigma$ (S/m) | $\varepsilon_r$ | $\sigma$ (S/m) |
| Skin | 1 | 38.97 | 2.47 | 38.52 | 2.51 |
| Brain | 7.5 | 46.68 | 3.02 | 461 | 2.97 |
| Tumor | $6 \times 6 \times 6$ | 64.05 | 4.18 | 65.1 | 3.96 |

The observed difference of approximately 11.38 dB between the two scenarios clearly indicates a significant variation in the reflection characteristics, which confirms the sensor's ability to detect the presence of a tumor effectively.

The observed differences between the simulated and measured results can be attributed mainly to the practical variations observed in real-world environments. First, minor discrepancies in the dielectric properties of the fabricated phantom materials arise from fabrication tolerances or compositional inconsistencies that can lead to deviations from ideal simulation parameters. Second, although simulations were conducted using perfectly defined geometries (spherical, cylindrical, and cubical tumor models), the actual fabricated tumor inevitably deviated from these ideal shapes. The experimental phantom shown in Figure 14(a) was deliberately designed with an irregular geometry to replicate a realistic human brain tumor more closely.

Nonetheless, the system consistently exhibits a pronounced $S_{11}$ variation between healthy and tumor conditions, approximately 14 dB in simulations and 11.38 dB in measurements, which affirms the strong sensitivity and reliability of the proposed microwave sensing system for noninvasive, real-time brain tumor detection.

## 5. COMPARATIVE ANALYSIS

Table 2 presents a performance comparison between the proposed brain tumor detection sensor and previously reported approaches in the literature, emphasizing the key benefits achieved in this work.

- The FSS integration with the antenna system in the proposed work delivers a notably higher peak gain of 8.3 dB, which surpasses those of [35–38]. This improved gain enables deeper and more effective penetration of electromagnetic energy into the cranial tissues, which improves both detection accuracy and overall system sensitivity.
- Experimental validation using a brain phantom revealed a pronounced $S_{11}$ variation of approximately 11.38 dB between healthy and tumorous cases, which demonstrates the superior detection sensitivity compared with the values reported in [36, 39–41].
- Moreover, unlike earlier studies that typically examined only a single tumor model, the present work conducted an extensive analysis across multiple tumor shapes and sizes, offering deeper insight into the correlation between geometry and sensor response.

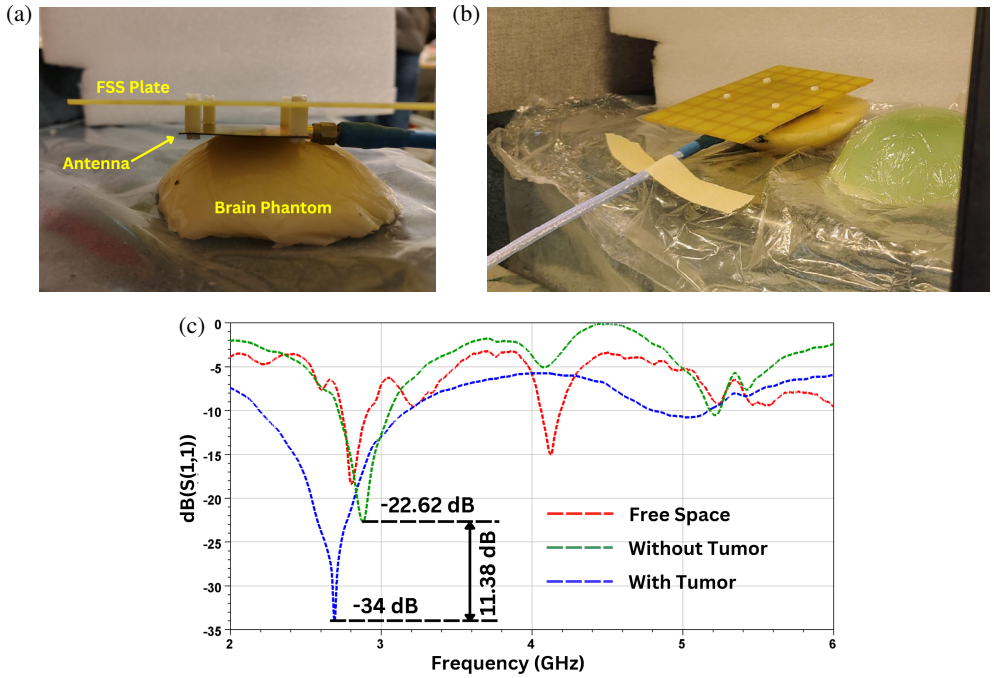


**FIGURE 14**. Measurement setup: (a) and (b) Antenna + FSS on phantom, (c) measured $S_{11}$ results.

**TABLE 2**. Comparative analysis.

| Ref. | Design | Size (mm) | Freq (GHz) | Gain (dB) | Application | Technique | Results |
|---|---|---|---|---|---|---|---|
| [39] | 4-element UWB-MIMO | 30 × 40 | 2.8–20 | - | Breast Tumor | Magnitude & Phase of $S_{11}$ to $S_{44}$ | Range of Min-Max variation in $S$-parameters |
| [35] | CP 4 × 1 Antenna Array | 200 × 78 × 1.5 | 2–3 | 6.6 | Kidney tumor | $\Delta f$, $\Delta S_{11}$ | $\Delta S_{11}$ variation & $\Delta f$ from 2 to 28 MHz for 4-stages of tumor |
| [36] | CSRR-SIW Antenna with cavity backing | 33 × 26 × 2 | 2.4 | 3.46 | Breast Tumor | $\Delta S_{11}$, Testing with phantom model, SAR | Variation of $S_{11}$ with various tumor sizes |
| [40] | DGS based Patch Antenna | 27.6 × 29.15 | 6.0–8.5 | - | Brain Tumor | Current Density | $\Delta S_{11}$ of 3.2 dB and variation in current density |
| [42] | Monopole Antenna | 14 × 10 × 0.805 | 0.3–0.5 | - | Kidney tumor | $\Delta f$, $\Delta S_{11}$ | $\Delta f$ of 11.2 MHz with tumor size 8076 mm$^3$ |
| [41] | FSS-backed Antenna | 36 × 35 × 0.51 | 4–5 | - | Brain Tumor | $\Delta S_{11}$ | $\Delta S_{11}$ of about 8 dB |
| [43] | 4 × 1 patch Array | 200 × 78 × 1.6 | 2.4 | - | Brain tumor | $\Delta S_{11}$ | Variation of 21.5 dB $\Delta S_{11}$ with tumor insertion |
| [37] | UWB with cross slots | 70 × 47 × 1.6 | 1.8–3 | 4.15 | Brain Cancer detection | Variation in $S_{21}$ & detection of echo state | Testing accuracy of 77.5% |
| [38] | 24-element array | 10 × 10 × 1.6 (Single antenna size) | 7.98/8.08 | 2.43 | Breast tumor | $Ex$ & $Ey$-field magnitude | With tumor addition: $Ex$ varies from 8.37 to 1.91 V/m. $Ey$ varies from 2.72 to 4.12 V/m |
| [44] | FSS loaded UWB antenna | Antenna- 29 × 20 × 1.6 FSS- 40 × 40 | 3.1–14.7 | 8.3 | Breast Tumor | Multiple antenna systems used to detect reflection & transmission coefficients | Variation in $\Delta S_{11}$, $\Delta S_{21}$ |
| This Work | FSS-backed Antenna | Antenna- 48 × 44 × 0.51 FSS- 120 × 90 × 1.6 | 2–3 | 8.3 | Brain tumor | $\Delta S_{11}$, testing with realistic phantom model, testing with various shapes | $\Delta S_{11}$ of about 11.38 dB with tumor presence |

Taken together, the combination of high gain, better $S_{11}$ sensitivity, and validation using realistic phantom models highlights the robustness, reliability, and clinical potential of the presented microwave sensor system for noninvasive brain tumor diagnostics.

## 6. CONCLUSION

This paper introduces a unique noninvasive approach to detecting the existence of a brain tumor by leveraging the variation of the $S$-parameter characteristics of an antenna. This is achieved by utilizing an FSS-backed antenna with high gain and directivity operating in the low frequency range of 1.5–3 GHz. The measurements were obtained by placing the designed antenna system close to the surface of the head. $S$-parameter variation can potentially be used to indicate the presence of tumors. First, the simulated results are presented using three layers: the Skin, Skull, and Brain. Tumors of different geometrical shapes were inserted in the brain area, and a simulated variation in $S_{11}$ characteristics was presented. These variations are adequate enough to indicate the presence of a tumor. Subsequently, an antenna system was fabricated, and the results were measured using a 3-D phantom model. The results validated the practical feasibility for potential use in noninvasive real-world brain tumor detection applications.

## REFERENCES


[1] Tariq, M., A. A. Siddiqi, G. B. Narejo, and S. Andleeb, "A cross sectional study of tumors using bio-medical imaging modalities," *Current Medical Imaging*, Vol. 15, No. 1, 66–73, 2019.

[2] Dessai, R., D. Singh, M. Sonkki, J. Reponen, T. Myllylä, S. Myllymäki, and M. Särestöniemi, "A breast tumor monitoring vest with flexible UWB antennas — A proof-of-concept study using realistic breast phantoms," *Micromachines*, Vol. 15, No. 9, 1153, Sep. 2024.

[3] Singh, D., E. Vihriälä, M. Särestöniemi, and T. Myllylä, "Microwave technique based noninvasive monitoring of intracranial pressure using realistic phantom models," in *Digital Health and Wireless Solutions*, 413–425, 2024.

[4] Särestöniemi, M., D. Singh, M. von und zu Fraunberg, and T. Myllylä, "Microwave technique for linear skull fracture detection — Simulation and experimental study using realistic human head models," *Biosensors*, Vol. 14, No. 9, 434, Sep. 2024.

[5] Alqadami, A. S. M., K. S. Bialkowski, A. T. Mobashsher, and A. M. Abbosh, "Wearable electromagnetic head imaging system using flexible wideband antenna array based on polymer technology for brain stroke diagnosis," *IEEE Transactions on Biomedical Circuits and Systems*, Vol. 13, No. 1, 124–134, 2019.

[6] Särestöniemi, M., D. Singh, C. Heredia, J. Nikkinen, M. von und zu Fraunberg, and T. Myllylä, "Digital twins for development of microwave-based brain tumor detection," in *Digital Health and Wireless Solutions*, 240–254, 2024.

[7] Winter, A., J. Laing, R. Paglione, and F. Sterzer, "Microwave hyperthermia for brain tumors," *Neurosurgery*, Vol. 17, No. 3, 387–399, Sep. 1985.

[8] Redr, J., T. Pokorny, T. Drizdal, O. Fiser, M. Brunat, J. Vrba, and D. Vrba, "Microwave hyperthermia of brain tumors: A 2D assessment parametric numerical study," *Sensors*, Vol. 22, No. 16, 6115, Aug. 2022.

[9] Dewhirst, M. W., B. L. Viglianti, M. Lora-Michiels, M. Hanson, and P. J. Hoopes, "Basic principles of thermal dosimetry and thermal thresholds for tissue damage from hyperthermia," *International Journal of Hyperthermia*, Vol. 19, No. 3, 267–294, 2003.

[10] Lyons, B. E., R. H. Britt, and J. W. Strohbehn, "Localized hyperthermia in the treatment of malignant brain tumors using an interstitial microwave antenna array," *IEEE Transactions on Biomedical Engineering*, Vol. 31, No. 1, 53–62, Jan. 1984.

[11] Särestöniemi, M., D. Singh, J. Reponen, and T. Myllylä, "Tailored 3D breast models for development of microwave based breast tumor screening," *Finnish Journal of eHealth and eWelfare*, Vol. 16, No. 1, 23–34, Apr. 2024.

[12] Benny, R., T. A. Anjit, and P. Mythili, "An overview of microwave imaging for breast tumor detection," *Progress In Electromagnetics Research B*, Vol. 87, 61–91, 2020.

[13] Muhammad, S. N., M. M. Isa, and F. Jamlos, "Review article of microwave imaging techniques and dielectric properties for lung tumor detection," in *AIP Conference Proceedings*, Vol. 2203, No. 1, 020012, 2020.

[14] Bensingh, V., J. B. J. J. Sheela, R. Krishnan, L. Kandasamy, and S. Devarajulu, "Detection of depth of the tumor in microwave imaging using ground penetrating radar algorithm," *Progress In Electromagnetics Research M*, Vol. 96, 191–202, 2020.

[15] Gong, Z., Y. Chen, X. Lin, and M. J. Cree, "Contrast-enhanced microwave cancer detection using angle-of-arrival approach," *IEEE Transactions on Antennas and Propagation*, Vol. 70, No. 5, 3772–3780, 2021.

[16] Sharma, S., D. Singh, M. Särestöniemi, T. Myllylä, and R. Kumar, "A frequency selective surface-backed microwave sensor for brain tumor detection," *International Journal of Microwave & Optical Technology*, Vol. 20, No. 5, 469–480, 2025.

[17] Rodriguez-Duarte, D. O., J. A. T. Vasquez, R. Scapaticci, L. Crocco, and F. Vipiana, "Brick-shaped antenna module for microwave brain imaging systems," *IEEE Antennas and Wireless Propagation Letters*, Vol. 19, No. 12, 2057–2061, Dec. 2020.

[18] Hossain, A., M. T. Islam, G. K. Beng, S. B. A. Kashem, M. S. Soliman, N. Misran, and M. E. H. Chowdhury, "Microwave brain imaging system to detect brain tumor using metamaterial loaded stacked antenna array," *Scientific Reports*, Vol. 12, No. 1, 16478, Oct. 2022.

[19] Hamza, M. N., M. T. Islam, and S. Koziel, "Advanced sensor for non-invasive breast cancer and brain cancer diagnosis using antenna array with metamaterial-based AMC," *Engineering Science and Technology, an International Journal*, Vol. 56, 101779, Aug. 2024.

[20] Hossain, A., R. Islam, M. T. Islam, P. Kirawanich, and M. S. Soliman, "FT-FEDTL: A fine-tuned feature-extracted deep transfer learning model for multi-class microwave-based brain tumor classification," *Computers in Biology and Medicine*, Vol. 183, 109316, Dec. 2024.

[21] Gupta, H., V. Maheshwari, and V. V. Thakery, "Brain tumor detection by microwave imaging using planner antenna," *International Journal of Bio-Science and Bio-Technology*, Vol. 8, No. 5, 201–210, 2016.

[22] Chandra, R. and I. Balasingham, "Detection of brain tumor and localization of a deep brain RF-source using microwave imaging," in *2015 9th European Conference on Antennas and Propagation (EuCAP)*, 1–5, Lisbon, Portugal, 2015.

[23] Asok, A. O., R. Anjaly, N. Kunju, and S. Dey, "Microwave medical imaging using a compact monopole antenna for brain tumor detection," in *2023 First International Conference on Microwave, Antenna and Communication (MAC)*, 1–4, Prayagraj,

India, Mar. 2023.

[24] Särestöniemi, M., D. Singh, R. Dessai, C. Heredia, S. Myllymäki, and T. Myllylä, "Realistic 3D phantoms for validation of microwave sensing in health monitoring applications," *Sensors*, Vol. 24, No. 6, 1975, Mar. 2024.

[25] Groumpas, E., M. Koutsoupidou, I. S. Karanasiou, C. Papageorgiou, and N. Uzunoglu, "Real-time passive brain monitoring system using near-field microwave radiometry," *IEEE Transactions on Biomedical Engineering*, Vol. 67, No. 1, 158–165, Jan. 2020.

[26] Hossain, A., M. T. Islam, S. K. A. Rahim, M. A. Rahman, T. Rahman, H. Arshad, A. Khandakar, M. A. Ayari, and M. E. H. Chowdhury, "A lightweight deep learning based microwave brain image network model for brain tumor classification using reconstructed microwave brain (RMB) images," *Biosensors*, Vol. 13, No. 2, 238, Feb. 2023.

[27] Sharma, S. and R. Kumar, "4-port MIMO antenna backed with frequency selective surface (FSS) for improved characteristics in n46 and n47 WLAN bands," *International Journal of Electronics*, Vol. 113, No. 1, 1–23, 2026.

[28] Mondal, R., P. S. Reddy, D. C. Sarkar, and P. P. Sarkar, "Investigation on MIMO antenna for very low ECC and isolation characteristics using FSS and metal-wall," *AEU — International Journal of Electronics and Communications*, Vol. 135, 153708, Jun. 2021.

[29] Sharma, S. and R. Kumar, "Compact frequency selective surface backed antenna for 24 GHz wearable applications," *Physica Scripta*, Vol. 100, No. 8, 085530, Aug. 2025.

[30] Watanabe, S.-I., H. Taki, T. Nojima, and O. Fujiwara, "Characteristics of the SAR distributions in a head exposed to electromagnetic fields radiated by a hand-held portable radio," *IEEE Transactions on Microwave Theory and Techniques*, Vol. 44, No. 10, 1874–1883, 1996.

[31] Elsheakh, D. M. N., A. M. Soliman, and E. A. Abdallah, "Low specific absorption rate hexa-band coplanar waveguide-fed planar inverted-F antenna with independent resonant frequency control for wireless communication applications," *IET Microwaves, Antennas & Propagation*, Vol. 8, No. 4, 207–216, Mar. 2014.

[32] Pokorny, T., D. Vrba, J. Tesarik, D. B. Rodrigues, and J. Vrba, "Anatomically and dielectrically realistic 2.5D 5-layer reconfigurable head phantom for testing microwave stroke detection and classification," *International Journal of Antennas and Propagation*, Vol. 2019, No. 1, 5459391, 2019.

[33] IT'IS Foundation, "Dielectric properties database," [Online]. Available: https://itis.swiss/virtual-population/tissue-properties/database/dielectric-properties/, Feb. 2026.

[34] IFAC, "Dielectric properties of body tissues," [Online]. Available: https://niremf.ifac.cnr.it/tissprop/htmlclie/htmlclie.php, Feb. 2026.

[35] Saleeb, D. A., R. M. Helmy, N. F. F. Areed, M. Marey, K. M. Almustafa, and A. S. Elkorany, "Detection of kidney cancer using circularly polarized patch antenna array," *IEEE Access*, Vol. 10, 78 102–78 113, 2022.

[36] Bhavani, M. V. L., D. Chaturvedi, T. Lanka, and A. Kumar, "Development of a QMSIW antenna sensor for tumor detection utilizing a hemispherical multilayered dielectric breast-shaped phantom," *IEEE Sensors Journal*, Vol. 24, No. 20, 32 080–32 089, Oct. 2024.

[37] Nair, V. V., E. George, and A. James, "Real-time tumor detection using electromagnetic signals with memristive echo state networks," *IEEE Internet of Things Journal*, Vol. 11, No. 20, 33 712–33 721, Oct. 2024.

[38] Moussa, M. N., M. A. Madi, and K. Y. Kabalan, "Breast tumor detection, sizing and localization using a 24-element antenna array," *IEEE Journal of Biomedical and Health Informatics*, Vol. 26, No. 10, 5109–5121, Oct. 2022.

[39] Sharma, M. K., M. Kumar, J. P. Saini, D. Gangwar, B. K. Kanaujia, S. P. Singh, and A. Ekuakille, "Experimental investigation of the breast phantom for tumor detection using ultra-wide band–MIMO antenna sensor (UMAS) probe," *IEEE Sensors Journal*, Vol. 20, No. 12, 6745–6752, Jun. 2020.

[40] Gupta, H. K., R. Sharma, and V. V. Thakre, "Tumor detection in multilayer brain phantom model by symmetrical-shaped dgs rectangular microstrip patch antenna," in *International Conference on Intelligent Computing and Smart Communication 2019*, 705–712, 2019.

[41] Sharma, S., D. Singh, M. Särestöniemi, T. Myllylä, and R. Kumar, "On-body FSS-backed high gain microwave system for brain tumor diagnosis," *Progress In Electromagnetics Research C*, Vol. 155, 245–254, 2025.

[42] Bouazizi, A., G. Zaibi, A. Iqbal, A. Basir, M. Samet, and A. Kachouri, "A miniaturized implantable monopole antenna design for kidney cancer detection," *World Journal of Modelling and Simulation*, Vol. 16, No. 1, 3–10, 2020.

[43] Saleeb, D. A., R. M. Helmy, N. F. F. Areed, M. Marey, W. M. Abdulkawi, and A. S. Elkorany, "A technique for the early detection of brain cancer using circularly polarized reconfigurable antenna array," *IEEE Access*, Vol. 9, 133 786–133 794, 2021.

[44] Ullah, N., Y. I. Abdulkarim, F. Wang, Y. Liu, F.-E. Zerrad, and M. Taouzari, "Detection of breast tumor with a frequency selective surface loaded ultra-wide band antenna system," *Physica Scripta*, Vol. 99, No. 8, 085543, 2024.